Lengths of ferroelectric domains: The role of defects and random fields

Uwe Voelker
Institut für Technische Physik, Deutsches Zentrum für Luft- und Raumfahrt, D-70569 Stuttgart, Germany

Kai Dinges, Urs Heine, and Klaus Betzler*
Fachbereich Physik, Universität Osnabrück, D-49069 Osnabrück, Germany
(Received 6 May 2010; published 7 June 2010)

Using noncollinear optical second-harmonic generation, the characteristic lengths of ferroelectric domains in strontium-barium niobate are determined. The role of the domain geometry in the random quasiphase matching process involved is elucidated by model calculations on different domain arrangements. The calculations prove that the domain geometries—especially the domain lengths—strongly affect the angular distribution of the generated second-harmonic light. The evaluation of the measured angular distributions in crystals with different doping concentrations shows that the domain lengths are distinctly albeit not drastically influenced by the dopant-induced random electric or strain fields.

DOI: 10.1103/PhysRevB.81.214104 PACS number(s): 77.80.Dj, 42.65.Ky, 42.70.Mp, 77.84.Ek

I. INTRODUCTION

Ferroelectric materials play an important role in nowadays and future applications such as, e.g., ferroelectric random access memories[1] or piezoelectric injection systems.[2] Many of their properties are affected by domain effects, thus a detailed knowledge of the domain geometry and the influencing factors is indispensable. As impurities can modify the material properties in both, positive and negative manner, it is of interest to identify the role of defects on the morphology of ferroelectric bulk domains. For this purpose, a defect-affine system is of advantage. A material class of special importance in this context are the so-called relaxor ferroelectrics, first described by Smolenskii.[3,4] Besides their relative permittivities usually exhibiting broad maxima in the temperature dependence,[5] they show additional interesting physical properties suitable for applications as, e.g., large electrostrictive effects.[6]

One of the most prominent members of the relaxors is strontium-barium niobate ($Sr_xBa_{1-x}Nb_2O_6$, SBN) due to its excellent photorefractive, electro-optic, nonlinear optic, and dielectric properties. These properties can be varied either by changing the composition x or by the inclusion of dopants. Thus SBN is most suitable both for many potential applications and for basic research in these fields. Despite numerous investigations, however, only few are known about the exact bulk-domain structure in SBN. Transmission electron micrographs reveal a "needlelike" geometry, at least in unpoled crystals, with the "needles" aligned along the crystal's polar axis.[7] The domain geometry at the polar-end faces measured by piezoelectric force microscopy shows a fractal-like pattern with a wide length scale.[8,9]

Recently it was shown that a random domain pattern can provide the k vectors necessary for momentum conservation in quasiphase matching geometries for second-harmonic generation in SBN.[10–12] The effect can be used for broadband harmonic generation[13,14] or for monitoring other integral properties like domain switching.[15,16] Furthermore, the typical features of the domain geometry show up in the angular distribution of the generated second-harmonic light. Evaluating this, *k-space spectroscopy* can be used to monitor the domain evolution during temperature or electric field treatment, which yielded a modified interpretation of the relaxor phase transition in SBN.[17,18]

Investigations of domain lengths in the above-mentioned transmission electron micrographs and by piezoelectric force microscopy reveal extensions in the direction of the crystallographic axis in the order of tens of microns.[19] Up to now, however, for the crystal bulk solely the domain *widths* are considered, assuming domain *lengths* to be equal to and limited by the crystal length. Only Kuznetsov *et al.*[20] assumed domains of limited shorter length, albeit only in a thin surface layer, not in the bulk of the crystal.

In the present paper, we show by model calculations that not only the domain widths but also the bulk-domain lengths are reflected in the angular distribution of the generated second-harmonic light in a fingerprintlike manner. From a fit to experimental data we can derive the typical domain lengths in pure and doped SBN.

II. MATERIAL PROPERTIES

SBN—$Sr_xBa_{1-x}Nb_2O_6$—crystallizes in an unfilled tetragonal tungsten-bronze structure over a broad composition range from $x=0.26$ to $x=0.87$ (Ref. 21) with the congruently melting composition at $x\approx 0.61$.[21,22] Throughout this tetragonal phase, SBN is ferroelectric at low temperatures (point group $4mm$, space group $P4bm$) and paraelectric at high temperatures (point group $4/mmm$, space group $P4/mbm$). The phase transition of SBN is of relaxor type (see, e.g., Ref. 5), i.e., distinctly broadened; the transition temperatures depend on the composition and vary from 290 K ($x=0.82$) to 500 K ($x=0.32$).[23] Dopants modify all properties distinctly, the phase-transition temperature, e.g., can be greatly varied by cerium and chromium[24] or by europium[25] or erbium.[26] Europium and erbium, furthermore, have been shown to broaden the phase-transition's temperature region.[25,26] Thus, the embedded rare-earth ions seem to increase the amount of random fields which are supposed to play a key role regarding the relaxor phase transition.[27]

Such an increase in randomness should also show up in the domain sizes. Consequently, we chose crystals doped

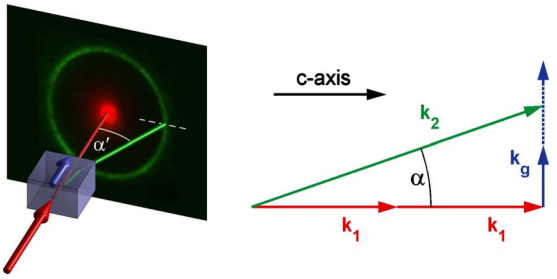

FIG. 1. (Color online) Experimental setup used (left) and momentum diagram for quasiphase matching (right). α and α' are internal and external cone angles, respectively. See text for details.

with different concentrations of erbium or europium for our investigations. The crystals were grown from the congruently melting composition using the Czochralski technique (for details see Ref. 21), undoped and doped with erbium or europium up to 1.14 mol %. They were cut to sizes of approximately $4\times4\times4$ mm^3 and polished to suit optical investigations. All experiments were carried out at room temperature.

III. EXPERIMENTAL ARRANGEMENT

The experimental setup for the determination of domain lengths is schematically sketched in the left part of Fig. 1. A laser beam (1064 nm, pulsed) is directed along the polar axis (c axis) of the investigated SBN crystal. A cone of second-harmonic light is generated due to the quasiphase matching scheme shown in the right part of Fig. 1. An image of a typically measured intensity profile of the light cone is displayed on the screen.

Momentum conservation is ensured through the additional momentum vector $\mathbf{k_g}$ which is provided by the Fourier representation of the "needlelike" domains in SBN (Ref. 11)

$$\sum \mathbf{k_i} = 0 \quad \text{or} \quad 2\mathbf{k_1} + \mathbf{k_g} - \mathbf{k_2} = 0. \tag{1}$$

Due to the elongation of the domains in c-axis direction, $\mathbf{k_g}$ is approximately perpendicular to this polar axis; the lengths of $\mathbf{k_1}$ and $\mathbf{k_2}$ are defined by the wavelengths and refractive indices of fundamental and harmonic beam. Thus a sharp internal cone angle

$$\alpha = \arccos\frac{2|\mathbf{k_1}|}{|\mathbf{k_2}|} \tag{2}$$

is forced if domains of infinite length are assumed. For finite-length domains this simple model requires some revision.

IV. MODEL CALCULATIONS

To account for finite domain lengths, we performed model calculations for different domain configurations. Two-dimensional domain geometries with variable domain lengths were constructed using Monte Carlo (MC) techniques. For this construction, lengths and widths of the domains were randomly chosen using normal distributions with

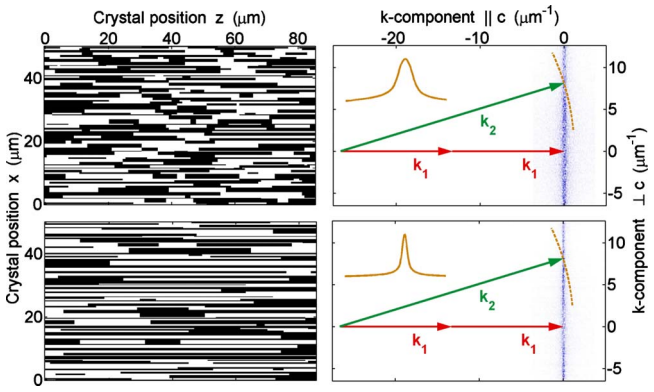

FIG. 2. (Color online) Left side: typical two-dimensional domain distributions, top: short domains, and bottom: long domains. Black and white denote the two possible domain orientations. Right side: corresponding density distributions of the momentum vector $\mathbf{k_g}$ (blue granulated).

certain mean values. Domain walls were assumed to be abrupt, furthermore, to be strictly parallel or perpendicular to the polar axis of the crystal. As long as the domain widths are considerably smaller than the domain lengths—which represents the "needlelike" geometry—only the amplitude, not the half width of the intensity profile is affected by the domain width. Thus it could be accomplished that the principal shape of the intensity profiles is not affected by the mean domain width but only by the domain length. The corresponding $\mathbf{k_g}$ distribution was calculated applying a two-dimensional Fourier transform on the domain configurations. The model can be extended to three dimensions using an appropriate three-dimensional MC construction and an according three-dimensional Fourier transform. As, however, no new aspects are gained which would warrant the considerably higher computing effort, we restricted our calculations to two dimensions.

Typical results are shown in Fig. 2—on the left side two of the domain geometries constructed, on the right side the corresponding $\mathbf{k_g}$ distributions plotted as density distributions of $\mathbf{k_g}$ end points (blue granulated). The relatively coarse granulation seen in the $\mathbf{k_g}$ distribution is due to the limited number of domains considered. Also plotted are the momentum vectors for a fundamental beam directed along the crystallographic c axis ($\mathbf{k_1}$) and for second-harmonic light ($\mathbf{k_2}$) quasiphase matched via a distinct $\mathbf{k_g}$ out of the distribution.

The inset bell-shaped curves in the right pictures of Fig. 2 denote the intensity profiles to be expected for the measured second-harmonic light as a function of the angle α (or α', respectively). To get these smooth curves, calculated $\mathbf{k_g}$ distributions for a large number of equivalent domain geometries are averaged, thus approaching the real case of a laser beam propagating through a larger three-dimensional crystal.

On the top the situation in a crystal with short domains is described—the distribution of the $\mathbf{k_g}$ vectors is broad, yielding a corresponding broad intensity profile. Compared to this, for a crystal with long domains (bottom pictures) the $\mathbf{k_g}$ distribution and thus the expected intensity profile is distinctly narrower.

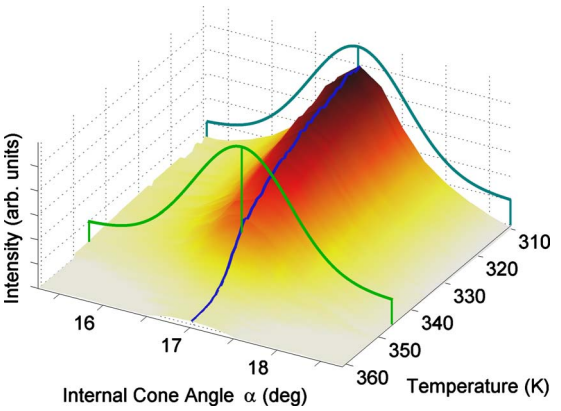

FIG. 3. (Color online) Temperature dependence of a typical intensity profile—intensity of the second-harmonic light as function of temperature and angle. The bell-shaped curves are Gaussian fits for the angular-intensity profiles at the respective temperatures. For a better visual comparison, the fit curves are normalized to the same height and slightly shifted upwards, as indicated. Also sketched is the temperature dependence of the intensity maximum (blue line) which denotes the intensity decrease toward the phase-transition region.

V. EXPERIMENTAL RESULTS

The intensity distribution in the second-harmonic light cones was measured by angular scans using an appropriate aperture combined with a photomultiplier and pulse processing electronics. The aperture was chosen small enough to have no effect on the shape of the intensity distribution. Furthermore, the data have been corrected for the influence of the Gaussian beam profile of the laser used.

To determine the influence of the crystal temperature on the domain sizes, the second-harmonic intensity as a function of temperature and cone angle, was measured. A typical result is shown in Fig. 3.

As evidenced by the two fit curves shown in Fig. 3, we found that—within the measurement's accuracy—the domain sizes do not show any dependence on temperature, at least at temperatures below and up to the phase-transition region. The decrease in the intensity when approaching the phase transition is due to the temperature dependence of the polarization inside the domains. This behavior of as-grown unpoled samples used in our investigations differs from that of electric field treated ones where a distinct dependence of the domain *sizes* on temperature was demonstrated.[18]

We, therefore, restricted our further evaluations on angular-intensity profiles measured at room temperature. Two typical intensity profiles are shown in Fig. 4. The expressed broadening for the doped crystal compared to the undoped hints on a decrease in the domain lengths caused by dopants.

The mean domain lengths can be derived from a fit of the model calculation to the experimental data. The corresponding fit curves for the two intensity profiles are also sketched in Fig. 4. In the fit procedure, the peak profiles and half widths of the intensity profiles were emphasized, more or less neglecting the side wings of the calculated curves. This is necessary as these side wings are typical artifacts of the

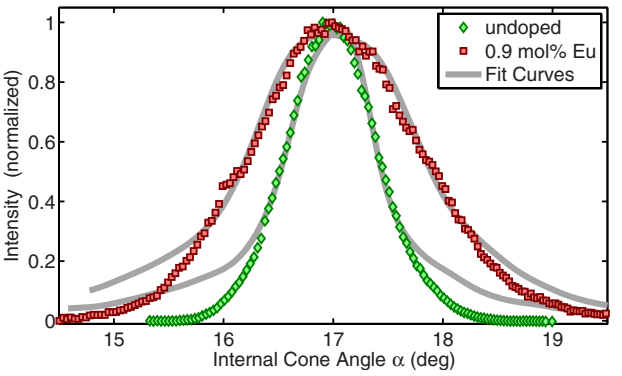

FIG. 4. (Color online) Intensity profile—intensity of the second-harmonic light as function of the cone angle α inside the crystal—for undoped and doped SBN.

Fourier transform caused by the steplike domain boundaries and by the limited overall field size.

To determine the dependence of the domain lengths on the doping concentration we measured the intensity profiles for a series of erbium- and europium-doped SBN crystals with doping concentrations ranging from 0 to 1.14 mol % and calculated the mean domain lengths from the fits to the model. The results are summarized in Fig. 5.

The mean domain lengths decrease from approximately 70 μm for undoped SBN to 40 μm for doping concentrations around 1 mol %. No significant difference is found between the two dopants chosen.

A fit formula proposed is also given in Fig. 5, it will be discussed in the following section.

VI. DISCUSSION

In a simple model one can assume that the domain length in unpoled ferroelectrics is determined or at least influenced by random fields or random charges. A respective model picture is sketched in Fig. 6.

In doped crystals, the density of such random charges should be proportional to the dopant concentration. Then their mean distance in the direction of the polar axis, which is related to the mean domain length, is proportional to the inverse cube root of the dopant concentration. Two extensions to this simple model are necessary.

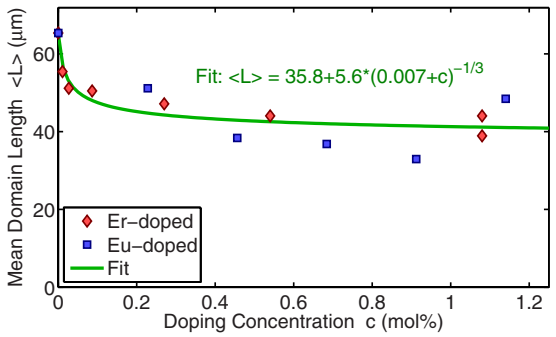

FIG. 5. (Color online) Mean domain lengths in SBN as a function of the doping concentration. The fit function includes the parameters derived from a fit of Eq. (3) to the experimental data.

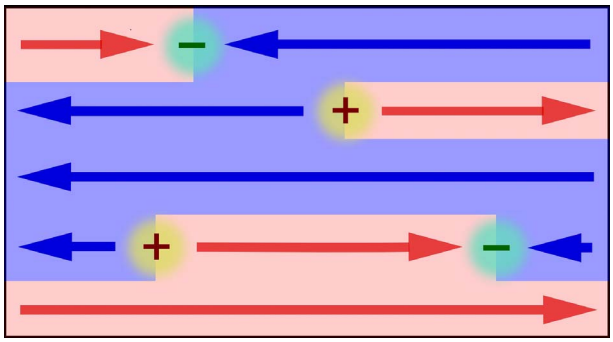

FIG. 6. (Color online) Model for the influence of random charges on the domain configuration in SBN.

(1) At finite temperatures, there must be a nonzero concentration of *intrinsic* random charges also in undoped crystals. These intrinsic random charges can be supposed to arise from the unfilled crystal structure, where in average one lattice site per unit cell is empty. The density of these intrinsic random charges can be introduced into the model by a corresponding dopant density c_i. (2) Due to energetic reasons, there must be an upper limit for the density of random charges with sufficient size, which defines a lower limit L_0 for the mean domain length.

We took the simplest mathematical description, including all the points discussed, to arrive at the fit expression for the mean domain length $\langle L \rangle$,

$$\langle L \rangle = L_0 + k(c_i + c)^{-1/3}. \tag{3}$$

The parameter c marks the dopant concentration which—as discussed above—controls the density of random charges. k is a proportionality factor for the influence of the dopant concentration on the domain length which also accounts for the fact that the dopant concentration in Eq. (3) is given in mole percent and not in $(\mu m)^{-3}$. A fit to the experimental data yields reasonable results as shown in Fig. 5. It should be noted that the density of *effective* random charges, i.e., such random charges which affect the domain length, is much less than the dopant concentration. This is consistent with the situation in pure crystals where—despite a large number of defects—the macroscopic lattice order is intact.

The result that the increase in the dopant concentration also leads to an increase in the random-charge-induced disorder also can explain the broadening of the SBN phase-transition temperature region with increasing dopant concentration.[25,26] Thus—despite their still controversially discussed role concerning the criticality of the phase transition,[28–30] dopant-induced random charges can be assumed to influence the geometry of the domains, especially the domain length, in a characteristic way.

ACKNOWLEDGMENTS

Support from the Graduate College *Nonlinearities of Optical Materials*, financed by the Deutsche Forschungsgemeinschaft and the Federal State of Niedersachsen, is gratefully acknowledged. We are much obliged to R. Pankrath and S. Podlozhenov for providing excellent-quality crystal samples.

*klaus.betzler@uos.de

[1] J. F. Scott and C. A. P. de Araujo, Science **246**, 1400 (1989).
[2] H. K. Suh, S. W. Park, and C. S. Lee, Fuel **86**, 2833 (2007).
[3] G. Smolenskii and V. Isupov, Zh. Tekh. Fiz. **24**, 1375 (1954).
[4] G. Smolenskii and A. Agranovskaia, Sov. Phys. Tech. Phys. **3**, 1380 (1958).
[5] L. E. Cross, Ferroelectrics **76**, 241 (1987).
[6] L. E. Cross, S. J. Jang, R. E. Newnham, S. Nomura, and K. Uchino, Ferroelectrics **23**, 187 (1980).
[7] D. Viehland, Z. Xu, and W. H. Huang, Philos. Mag. A **71**, 205 (1995).
[8] P. Lehnen, W. Kleemann, T. Woike, and R. Pankrath, Phys. Rev. B **64**, 224109 (2001).
[9] J. Dec, V. V. Shvartsman, and W. Kleemann, Appl. Phys. Lett. **89**, 212901 (2006).
[10] S. Kawai, T. Ogawa, H. S. Lee, R. C. DeMattei, and R. S. Feigelson, Appl. Phys. Lett. **73**, 768 (1998).
[11] A. R. Tunyagi, M. Ulex, and K. Betzler, Phys. Rev. Lett. **90**, 243901 (2003).
[12] J. Trull, C. Cojocaru, R. Fischer, S. M. Saltiel, K. Staliunas, R. Herrero, R. Vilaseca, D. N. Neshev, W. Krolikowski, and Y. S. Kivshar, Opt. Express **15**, 15868 (2007).
[13] J. J. Romero, C. Arago, J. A. Gonzalo, D. Jaque, and J. G. Sole, J. Appl. Phys. **93**, 3111 (2003).
[14] R. Fischer, S. M. Saltiel, D. N. Neshev, W. Krolikowski, and Y. S. Kivshar, Appl. Phys. Lett. **89**, 191105 (2006).
[15] D. V. Isakov, M. S. Belsley, T. R. Volk, and L. I. Ivleva, Appl. Phys. Lett. **92**, 032904 (2008).
[16] T. Volk, D. Isakov, M. S. Belsley, and L. Ivleva, Phys. Status Solidi A **206**, 321 (2009).
[17] U. Voelker and K. Betzler, Phys. Rev. B **74**, 132104 (2006).
[18] U. Voelker, U. Heine, C. Gödecker, and K. Betzler, J. Appl. Phys. **102**, 114112 (2007).
[19] V. V. Shvartsman, W. Kleemann, T. Lukasiewicz, and J. Dec, Phys. Rev. B **77**, 054105 (2008).
[20] K. A. Kuznetsov, G. K. Kitaeva, A. V. Shevlyuga, L. I. Ivleva, and T. R. Volk, JETP Lett. **87**, 98 (2008).
[21] M. Ulex, R. Pankrath, and K. Betzler, J. Cryst. Growth **271**, 128 (2004).
[22] K. Megumi, N. Nagatsuma, Y. Kashiwada, and Y. Furuhata, J. Mater. Sci. **11**, 1583 (1976).
[23] C. David, T. Granzow, A. Tunyagi, M. Wöhlecke, T. Woike, K. Betzler, M. Ulex, M. Imlau, and R. Pankrath, Phys. Status Solidi A **201**, R49 (2004).
[24] T. Granzow, T. Woike, W. Rammensee, M. Wöhlecke, M. Imlau, and R. Pankrath, Phys. Status Solidi A **197**, R2 (2003).
[25] A. Andresen, A.-N. Bahar, D. Conradi, I.-I. Oprea, R. Pankrath, U. Voelker, K. Betzler, M. Wöhlecke, U. Caldiño, E. Martín, D.

Jaque, and J. García Solé, Phys. Rev. B **77**, 214102 (2008).
[26] I.-I. Oprea, U. Voelker, A. Niemer, R. Pankrath, S. Podlozhenov, and K. Betzler, Opt. Mater. **32**, 30 (2009).
[27] W. Kleemann, J. Dec, P. Lehnen, R. Blinc, B. Zalar, and R. Pankrath, Europhys. Lett. **57**, 14 (2002).
[28] W. Kleemann, J. Mater. Sci. **41**, 129 (2006).
[29] J. F. Scott, J. Phys.: Condens. Matter **18**, 7123 (2006).
[30] W. Kleemann, J. Phys.: Condens. Matter **18**, L523 (2006).